Acute myeloid leukemia cells are targeted by the naturally occurring CXCR4 antagonist EPI-X4

Lisa M. Kaiser[1], Mirja Harms[2], Daniel Sauter[2,3], Vijay PS Rawat[1,4], Mirco Glitscher[5], Rüdiger Groß[2], Eberhard Hildt[5], Jan Münch[2], Christian Buske[1,*]

[1]Comprehensive Cancer Center Ulm, Institute of Experimental Cancer Research, University Hospital Ulm, Ulm, Germany;

[2]Institute of Molecular Virology, Ulm University Medical Center, Ulm, Germany

[3]Institute for Medical Virology and Epidemiology of Viral Diseases, University Hospital Tübingen, 72076 Tübingen, Germany

[4]Special Centre for Molecular Medicine, Jawaharlal Nehru University, Delhi 110067, India

[5]Department of Virology, Paul-Ehrlich-Institute, Langen, Germany

*corresponding author:

Christian Buske M.D.

CCC Ulm, University Hospital Ulm

Institute of Experimental Cancer Research

University Hospital Ulm, Germany

E-Mail: christian.buske@uni-ulm.de

Running title: Targeting of AML by EPI-X4

Abstract

The G protein-coupled receptor (GPCR) and chemokine receptor CXCR4 plays an essential role in tumor initiation and maintenance. This is exemplified in acute myeloid leukemia (AML), where CXCL12-mediated CXCR4 signaling plays a pivotal role for the crosstalk between leukemic stem cells and their microenvironmental niche. Despite the key role of CXCR4 in cancer, surprisingly little is known about endogenous mechanisms that specifically target CXCR4 and dampen its activity. Here, we demonstrate that the naturally occurring peptide and CXCR4 antagonist EPI-X4 and its optimized derivatives effectively blocks CXCL12-mediated migration of AML cells towards a CXCL12 gradient and impairs growth of AML cells *in vitro* and *in vivo* in contrast to normal hematopoietic stem and progenitor cells. This anti-leukemic activity of EPI-X4 was accompanied by suppression of CXCR4-mediated MAPK signaling. Of note, EPI-X4 suppressed metabolic pathways and induced depletion of intracellular nicotinamide phosphoribosyltransferase (iNAMPT) in AML cells, linking anti-CXCR4 activity to shifts in NAD+ metabolism.

Introduction

G protein-coupled receptors (GPCRs) represent the largest family of membrane receptors with an estimated number of 800 members in humans. Several GPCRs are known to be critically involved in tumorigenesis [1,2]. Although GPCRs are targets for approximately 30% of all marketed drugs, only a very limited number of agonists or antagonists acting through these receptors are currently used for cancer therapy [2]. In addition, very little is known about naturally occurring peptides limiting the activities of GPCRs and representing a promising resource for the development of new GPCR antagonists. The C-X-C chemokine receptor type 4 (CXCR4) has been recognized as a key regulator for cancer growth and invasion for a long time and has emerged as a promising target for anti-cancer drugs [3]. CXCR4 is a classical GPCR belonging to the Rhodopsin-like class A subfamily with CXCL12 as its only endogenous chemokine ligand Within the hematopoietic system, CXCR4 is expressed on most cell types including lymphocytes, stromal fibroblasts, endothelial and epithelial cells, as well as hematopoietic stem cells and cancer cells [4]. CXCR4 controls stem cell retention in the adult bone marrow (BM) and its disruption leads to a release of the hematopoietic stem cell (HSC) pool with the ability to restore normal blood cell population. CXCR4 has been associated with carcinogenesis, and elevated CXCR4 levels have been portrayed in numerous cancers with relation to poor prognosis and therapy resistance [5]. In hematological malignancies, high expression of CXCR4 is observed in several entities, ranging from acute leukemias such as acute lymphoblastic leukemia (ALL) and acute myeloid leukemia (AML) to a variety of malignant lymphomas including chronic lymphocytic leukemia (CLL), diffuse large B cell lymphoma (DLBCL), follicular lymphoma (FL), marginal zone lymphoma (MZL), hairy cell leukemia (HCL) and mantle cell lymphoma (MCL) [6].

Among all these hematological malignancies, CXCR4 is particularly prominent in AML: in AML, malignant cells are propagated and maintained by so called leukemic stem cells (LSCs), which are dependent on the crosstalk with the BM-niche mediated by CXCL12-CXCR4 signaling. Blockage of this axis is highly effective in dislodging leukemic cells from their protective BM niches. *Vice versa*, overexpression of CXCR4 on LSCs is one of the key mechanisms

promoting BM anchoring and quiescence of leukemic cells via its interaction with CXCL12. By this, cytotoxic effects of chemotherapies including targeted approaches such as Flt3 inhibitors are impaired in experimental systems [7].

Based on all this, it is not surprising that there are major efforts to develop compounds targeting CXCR4, and clinical testing of CXCR4 antagonists has been reported amongst others in AML and Waldenström's Macroglobulinemia (WM) [8]. In this context it is, however, surprising that little is known about naturally occurring mechanisms able to counteract the evolutionarily highly conserved CXCR4 effects and to dampen CXCR4 signaling *in vivo* in normal but also in malignant hematopoiesis. Here we demonstrate for the first time that the naturally occurring CXCR4 antagonist EPI-X4 impairs AML cell growth in a cell intrinsic way, suppressing CXCR4-mediated signaling and stem cell associated gene expression. Of note, EPI-X4 interfered with metabolism, inducing rapid and profound loss of intracellular NAMPT, a key regulator of energy metabolism, and suppression of metabolic pathways such as glycolysis and cholesterol biosynthesis [9].

Results

EPI-X4 and its optimized derivatives impair migration and growth of AML cells *in vitro* and *in vivo*

We first evaluated CXCR4 expression in functionally validated LSCs, characterized by their ability to induce AML in transplanted NSG mice, transcription of *CXCR4* was readily detectable in the LSC as well as in the non-LSC compartment (Fig.1A).

To investigate a potential role of the natural CXCR4 antagonist EPI-X4 in AML, we first tested its ability to bind to and to block CXCR4 antibody binding on AML cells. Efficient and dose-dependent blocking of CXCR4 by EPI-X4 and by optimized derivatives (WSC02 and JM#21, respectively), generated by structure-activity-relationship (SAR) studies and subsequent synthetic modulation inserting mutations [10,11], was documented in antibody competition assays, using two different antibody clones recognizing the 1D9 and 12G5 epitopes. Efficient blockage of the 12G5 epitope was achieved at a concentration of 200 µM of EPI-X4 confirming previous results [11]. In contrast, EPI-X4 did not block the 1D9 epitope showing that the CXCR4 N-terminus is not involved in receptor binding. The activity optimized EPI-X4 derivatives WSC02 and JM#21 achieved an efficient blockage of 12G5 at a concentration of 10 µM (Fig. 2A). In contrast, the 1D9 epitope was also not affected by the compounds, as expected (Fig. 2B).

As illustrated in Fig. 2C, EPI-X4 and its optimized derivative WSC02 were able to impair growth of the NPM1 mutated OCI-AML3 cell line by 66 and 72 %, respectively, compared to the inactive control peptide. The ability to impair migration of AML cells towards a CXCL12 gradient *in vitro* was tested using a transwell assay: EPI-X4 reduced migration by 74% compared to the inactive control peptide (Alb409-423) at a concentration of 200 µM. The optimized derivatives WSC02 and JM#21 efficiently blocked migration of AML cells by 74 % and 98 %, respectively, at a concentration of 10 µM compared to the inactive control peptide (Fig. 2D-E).

To test the impact of EPI-X4 and its derivatives on AML behavior *in vivo*, primary AML cells were treated with the CXCR4 antagonists *in vitro* and subsequently transplanted into NSG mice: EPI-X4 as well as its derivatives nearly completely blocked homing of AML cells. In addition, long-term engraftment of primary AML cells was significantly impaired by EPI-X4 and its optimized forms, indicating that the CXCR4 antagonists can act at the level of AML LSCs (Fig. 3A-B). Importantly, these peptides had no inhibitory effect on CD34+ normal stem and progenitor cells, pointing to a differential effect of EPI-X4 on normal versus leukemic stem cells (Fig. 3C).

EPI-X4 and its optimized derivatives suppress CXCR4 mediated MAPK signaling

To understand the mechanisms underlying the inhibitory effect of EPI-X4 and its optimized derivatives, we determined whether the CXCR4 antagonists suppressed known downstream signaling pathways such as ERK signaling in AML cells. To this end, we monitored ERK phosphorylation at Tyr204 (ERK1) and Tyr187 (ERK2) in OCI-AML3 cells after CXCL12 stimulation using flow cytometry. EPI-X4 had no major effect on ERK phosphorylation in contrast to the optimized derivatives WSC02 and JM#21, which were able to suppress phosphorylation significantly in a dose–dependent manner, with JM#21 showing the strongest effect. These results were validated by Western blot (Suppl. Fig.1). Similar results were obtained for phosphorylation of AKT at Ser473 (Fig.4 A-B).

Next, we investigated the effect of EPI-X4 on the global kinase activity of OCI-AMl3 cells after stimulation with CXCL12 using PamChip technology. In line with the effects on MAPK phosphorylation seen by FACS and Western blotting for the EPI-X4 derivatives, EPI-X4 suppressed the activation of different members of the MAPK signaling cascade, including p38, ERK1 and ERK2 (Fig. 5A). The kinome analysis also revealed that suppression of kinases by EPI-X4 extended to both tyrosine kinases, as well as serine/threonine kinases such as PIM1 and PIM3 or (Fig.5B-C). Of all kinases analyzed, the PIM1/3 serine/threonine kinases were among those with the highest specificity score and were robustly downregulated by all EPI-X4 derivatives tested (Suppl. Figure. 2).

EPI-X4 suppresses metabolic pathways and induces depletion of intracellular NAMPT in AML cells

To further assess the effect of EPI-X4 at the molecular level, we performed RNA-Seq. Incubation of OCI-AML3 cells with EPI-X4 or the inactive control for 24 h induced differential expression of 1047 genes (FDR<0.05) (1645 upregulated and 840 downregulated genes) (Suppl. Table 2). Among the top downregulated genes was *CD300A*, a cell surface glycoprotein that plays a role in angiogenesis and has been reported to promote tumor progression in AML [12]. In addition, *CD109* was among the top downregulated genes. This gene is associated with stemness and belongs to a 4-gene expression signature predicting adverse outcome in patients with AML and high level of *Wilms Tumor-1* (*WT1*) gene expression [13] (Suppl. Table 2). Strikingly, there was a strong enrichment for genes involved in metabolism among the downregulated gene sets. This was also reflected in the Enrichr pathway analysis with prominent downreguation of the pathways “Glycolysis” and “Cholesterol Biosynthesis” (Fig. 6A) (Suppl. Table 3). Affected genes included key players in carbohydrate metabolism such as hexokinase 1 (HK1), Aldolase, Fructose-Bisphosphate C (ALDOC) or Enolase 1 and 2 (ENO 1/2), but also main regulators of fatty acid synthesis and cholesterol biosynthesis (Fig. 6B). Upregulated pathways were enriched for genes involved in p53 regulation (Suppl. Table 4).

To further assess the protein profile of EPI-X4 treated AML cells, we performed proteomic analysis using tandem mass spectrometry. EPI-X4 induced differential expression of 122 proteins (108 down and 14 proteins up). Similar to the transcriptome data, pathway analysis demonstrated a significant downregulation of metabolic pathways involved in energy metabolism such as glycolysis, oxidative phosphorylation, amino acid metabolism or the citric acid cycle (Fig. 7). Upregulated pathways recurrently emerging were FAS, TP53, Ubiquitin proteasome and DNA repair/DNA damage pathway (Fig. 7).

Of note, nicotinamide phosphoribosyltransferase (NAMPT), one of the major determinants of the cellular energy metabolism, was among the top 5 differentially expressed proteins in AML,

with a robust and reproducible downregulation in independent experiments using LC-MS (Fig. 8A). This was confirmed by Western blotting for NAMPT (Fig. 8B), which also demonstrated downregulation by the optimized derivatives, AMD 3100 and the known NAMPT inhibitor FK-866. Importantly, this was not accompanied by changes in the intracellular NAD+ content in contrast to treatment with the NAMPT inhibitor FK-866 serving as a positive control (Suppl. Fig. 3). When we quantified intracellular (iNAMPT) over 24 h, harvesting protein every two hours, we observed a decrease of iNAMPT in the presence of EPI-X4 at 8 h and in the presence of JM#21 at an even earlier time point (Fig. 8C). This effect could be counteracted by adding recombinant NAMPT to the cells (Fig. 8D). Of note, co-incubation of the cells with EPI-X4 and the proteasome inhibitor Bortezomib did not prevent decrease of iNAMPT as seen via Western blot, suggesting that the CXCR4 antagonist did not reduce intracellular protein levels via proteasome-mediated protein degradation (data not shown). Interestingly, when we tested NAMPT protein levels in normal HSPCs after treatment with the anti-CXCR4 compounds, we did not observe a decrease in intracellular NAMPT (Fig. 8E).

Based on this we tested whether NAMPT is secreted upon CXCR4 blocking, thereby diminishing the intracellular NAMPT pool. Life cell imaging on OCI-AML3 cells transduced with NAMPT cloned into a GFP-reporter vector in OCI-AML3 cells revealed a substantial decrease of intracellular GFP positivity over time upon treatment with EPI-X4 or JM#21. This was accompanied by an increase of GFP+ extracellular particles using nanoparticle tracking videomicroscope (Zetaview) with a 1.5- and 2.5-fold increase for EPI-X4 or JM#21, respectively, as compared to the inactive peptide control (Fig. 8F-G). Brefeldin treatment had no effect on the decrease of intracellular NAMPT confirming other reports demonstrating that its release is independent of a classical ER–Golgi-dependent pathway [14]. In contrast, Chloroquin and Trichostatin induced substantial loss of iNAMPT as previously observed in other studies, indicating that iNAMPT release upon CXCR4 blocking is an acetylation-dependent mechanism and lysosomal trafficking might be involved (data not shown) [14].

Discussion

The key role of the bone marrow microenvironment for maintaining growth of AML cells is known for a long time [15-17]. This crosstalk is depending on a complex interplay between the leukemic cells and the BM stromal cells mediated by ligand – receptor interactions, involving multiple molecules [18]. Among these, CXCR4 has been recognized to be vital for leukemic growth, and the concept to impair AML growth by interfering with the CXCR4 – CXCL12 crosstalk has been tested in clinical trials using the CXCR4 antagonist AMD3100 [19,20]. Importantly, the CXCR4 – CXCL12 crosstalk is evolutionarily highly conserved and is not restricted to leukemic cells, but also vital for homing and migration of normal hematopoietic stem cells and stem cells of multiple other organs. Based on this, it will be fundamental for the organism to control the CXCR4-CXCL12 crosstalk to maintain normal stem cell homeostasis and to avoid abundant mobilization of HSCs as observed after treatment with the CXCR4 antagonist AMD3100 in experimental models and in patients [21,22]. Despite the overall well recognized relevance of CXCR4 for HSC and LSCs behavior, little is known about naturally occurring mechanisms, which are able to specifically dampen CXCR4 activity and to counteract CXCR4-mediated homing of HSCs and LSCs to their microniche. It is known that CXCR4 activity is positively controlled at the transcriptional level by the Nuclear Respiratory Factor-1 (NRF-1) and negatively by Ying Yang 1 (YY1) [23]. Furthermore, multiple factors have been shown to increase CXCR4 activity such as IL-2, IL-4, IL-7, IL-10, IL-15, and TGF-1β [24] or to suppress activity in the case of TNF-α, INF-γ, and IL-1β [25]. However, all these mechanisms are not highly specific for CXCR4. Of note, this also holds true for the widely used CXCR4 antagonist AMD3100, which functions as an allosteric agonist of CXCR7, being able to induce the recruitment of β-arrest into CXCR7 [26]. In this context, it is noteworthy that the CXCR4 ligand CXCL12 binds to CXCR7 with an even 10-fold higher affinity compared to CXCR4 [27]. Taking all this into account, it is remarkable that with EPI-X4 a highly specific CXCR4 inhibitor exists, which is able to impair AML growth in a variety of experimental read-outs. One of the intriguing results is that EPI-X4 and its optimized derivatives impaired AML growth independently of the microenvironment as in all assays AML cells were cultured without any bystander cells in

serum free conditions. EPI-X4 and its derivatives were able to significantly impair migration towards a CXCL12 gradient, clonogenic growth, but also engraftment into NSG mice after *in vitro* incubation, the latter indicating that EPI-X4 is able to act at the level of LSCs. All this indicates that EPI-X4 can act cell-intrinsically and is not depending on the BM niche. These observations are in line with a recently published report, in which CXCR4 was identified as key regulator of myeloid leukemogenesis in mice using an *in vivo* CRISPR screen. Interestingly, CXCL12 was dispensable for leukemia development, whereas CXCR4 signaling was essential for AML cells preventing their differentiation. Importantly, these data demonstrate that beyond its role in mediating crosstalk to the microenvironment, CXCR4 acts also cell-intrinsically, triggering key signaling cascades promoting and maintaining the malignant phenotype of the cell [28]. As expected, EPI-X4 impaired phosphorylation of the MAPK pathway, documented by FACS and PAMChip-based quantification of phosphorylation of members of this pathway and validated by Western blot. Surprisingly, however, RNA-Seq and proteomics demonstrated that EPI-X4 was able to suppress preferentially and robustly metabolic pathways such as glycolysis and cholesterol biosynthesis, which belonged to the top downregulated pathways using different tools for pathway analysis. Thus, beside downregulation of CXCR4–dependent signaling, our data point to another yet unknown effect of EPI-X4 and that is to change metabolism, linking its anti-cancer activity to metabolic shifts. These alterations in metabolism seem not to be cancer subtype-specific as we observed the modulation of metabolic pathways also in WM, an indolent B-cell lymphoma, for which activating CXCR4 mutations are a major driver of tumor growth [3,29]. In recent years, there has been growing interest into metabolism of cancer, also with the aim to identify metabolic vulnerabilities in malignant cells. NAMPT is the rate limiting enzyme involved in the conversion of nicotinamide into nicotinamide monophosphate, which generates NAD+, which itself is essential for OXPHOS and the TCA cycle as well as glycolysis. Thus, availability of NAMPT is a major determinant of the energy household of the cell [9]. NAMPT overexpression has been described in cancer cells, and pharmacological NAMPT targeting has shown anti-tumor effects in AML and WM, indicating addiction to nicotinamide metabolism in these cancers [30,31,32]. Just recently, resistance to

Venetoclax/Azacytidine in AML has been linked to increased nicotinamide metabolism at the level of AML LSCs [33]. Intriguingly, we saw substantial loss of intracellular NAMPT (iNAMPT) upon EPI-X4 incubation. This loss seemed not to be due to accelerated proteasome-mediated degradation as the inhibitor Bortezomib did not affect iNAMPT loss of EPI-X4 treated cells. Instead, live cell imaging experiments suggest that EPI-X4 induces increased secretion of iNAMPT. Secretion of NAMPT is a phenomenon known from a variety of tissues. It has been shown that iNAMPT secretion is regulated by SIRT1-mediated deacetylation in adipose tissue and that extracellular NAMPT (eNAMPT) is circulating in extracellular vesicles in mice [34,35]. Our observation that EPI-X4 or its derivatives impair AML LSCs, but spare normal HSCs in our NSG transplantation assays, suggests that EPI-X4 induces different metabolic alterations in leukemic versus normal HSCs or that LSCs are more addicted to certain pathways than healthy HSCs. This would imply that preferentially targeting of LSCs compared to HSPCs by EP-X4 is mediated at least in part via metabolism.

In summary, our data demonstrate that a naturally occurring CXCR4 antagonist is able to interfere cell intrinsically with AML growth mediated by impairing CXCR4 downstream signaling but also by suppressing metabolic pathways and depleting intracellular NAMPT. In addition, they underline, that endogenous peptides can serve as tool box to develop optimized derivatives with pre-clinical anti-leukemic activity and drug potential.

Materials and Methods

Quantification of CXCR4 surface levels by flow cytometry

All cell line experiments were conducted under serum-free conditions (RPMI plus 1% penicillin/streptomycin). Cells were incubated with different CXCR4 antagonists or an inactive control peptide at different concentrations as indicated for 30 min at 4 °C. A control sample was incubated with PBS only to determine basal receptor levels at the cell surface. After incubation, cells were stained with anti-CXCR4 antibodies (APC-labeled 12G5 antibody, 555976 or PE-labeled 1D9 antibody, 551510 from BD Biosciences).

Inhibition of ERK and AKT signaling by EPI-X4 and its optimized derivatives in AML cells

Inhibition of ERK and AKT signaling was performed as previously described [29]: briefly, cells were seeded in 100 µl starvation medium (RPMI, 1% FCS) and starved for 2 hours. 5 µl compound in PBS was added and cells were further incubated for 15 min. Afterwards, 5 µl CXCL12 (100 ng/ml final concentration on cells) was added for 2 min before the reaction was stopped by adding PFA and shifting to 4°C. After 15 min, medium was removed by centrifugation and cells permeabilized by adding ice cold MetOH for 15 min. Cells were then washed and the first antibody was added (phospho-p44/42 MAPK (Erk1) (Tyr204)/ (Erk2) (Tyr187) (D1H6G) mouse mAb (cell signaling, #5726) and phospho-Akt (Ser473) (193H12) rabbit mAb (cell signaling, #4058)) for 2 hours and stained with adequate secondary antibody afterwards. Cells were analyzed by flow cytometry with FACS Cytoflex.

CFC assay

Colony forming cell unit assay was performed as follows: $1x10^6$ cells were seeded in 1 ml serum free medium and treated with the indicated compounds. After 24 h, a 1:300 dilution was prepared and approximately. 300 cells were plated per dish (Methocult H4330 StemCell Technologies). Colonies were scored on day 7 after plating.

Migration

OCI-AML3 cells were seeded together with EPI-X4, WSC02, JM#21 or an inactive control peptide control in the upper well of a transwell. 10 nM CXCL12 was supplemented to the lower chamber. After 2 h incubation at 37°C, 5% CO_2, cells that had migrated to the lower compartment were analyzed using the CellTiter-Glo Luminescent Cell Viability Assay according to the manufacturer's instructions. Percentage of specific migration was calculated using the following formula: % migration = ((specific migration-unspecific migration)/total cells) *100.

RNA-Sequencing

OCI-AML3 cells were cultured in medium without FBS containing 200 µM of either the inactive peptide or EPI-X4. After 24 h, cells were collected, and RNA was isolated using the RNA isolation Kit Direct-zol RNA MiniPrep according to the manufacturer's protocol. After quality check, the RNA was prepped using the TruSeq RNA sample Kit from Illumina, and samples were run on the Illumina HiSeq 2000 sequencer. Afterwards, alignment was performed, and gene expression was analyzed by basepair.

Proteomics

Mass spectrometry was performed by the Core Unit Mass Spectrometry and Proteomics using Tandem mass spectrometry (LCMS). The protein for analysis was prepared as follows: $10x10^6$ were treated with 200 µM of either EPI-X4 or the inactive control in serum-free conditions for 24 h. Cells were washed with ice-cold PBS and the pellet was subsequently frozen down at -80.

Quantification of NAMPT protein levels

For Western blot analysis, OCI-AML 3 cells or normal HSPCs were counted and $2x10^6$ cells were cultured in 12 well plates in medium without FBS containing 200 µM of either the inactive peptide or EPI-X4, 10 µM WSC02, JM#21, AMD3100 or FK-866 proteins were isolated using 100-200 µl ice cold M-PER lysis buffer with Halt™ Protease and Phosphatase Inhibitor Cocktail. Equal amounts of total protein were loaded on a gel and separated using 8 – 16% SDS-PAGE gels, PVDF membranes were blotted using semi-dry Trans-Blot® Turbo™ Transfer System and analyzed using anti-NAMPT (1:200) monoclonal antibody (Santa Cruz).

Kinome profiling

Cells were treated with either EPI-X4 (200µM), WSC02 (10µM), JM#21 (10µM) or AMD3100 (10µM) and CXCL12 (10nM) or CXCL12 (10nM) PBS control for 10 minutes in serum free conditions. Cell lysis was achieved via the M-PER™ Mammalian Protein Extraction Reagent (78503, Thermo Scientific), which was supplemented with Halt™ Protease Inhibitor Cocktail (87785, Thermo Scientific) and Halt™ Phosphatase Inhibitor Cocktail (78420, Thermo Scientific). Qubit was used to determine protein concentrations in samples. Assessment of serine-/threonine-kinases (STK)- and Tyrosine (PTK) activity was measured in a PamStation 12 instrument under use of the Evolve software (PamGene International BV). Reactions were supplemented with 400 µM ATP and 2 µg (STK) or 5 µg (PTK) total protein. Porous aluminum oxide arrays containing 144 different 13-mer peptides being substrate to STKs or PTKs served as reaction matrix. Measurement of phosphorylated peptides was performed via imaging of FITC-labeled, phosphosite-specific antibodies with a CCD camera Quantification of resulting signal intensities was performed using the BioNavigator 6 ® software (BN6, PamGene International BV) with subsequent log2-transformation. Herein, a putative list of active kinases was predicted based on phosphorylated peptides using the functional scoring tool Upstream Kinase Analysis (BN6).

Stable transduction of OCI-AML3 cells

Retroviral particles were generated by cotransfecting Lenti-X™ 293T cells with the lentiviral vector pCDHMSCV-EF1-GFP-T2A-PURO expressing NAMPT, the packaging plasmid pSPAX2, and VSV-G encoding pMD2.G, using TransIT®-LT1. Cells containing constructs or empty vector control were sorted on a BD FACSAria™ III for the fluorescence marker GFP expressed from pCDH-MSCV-EF1-GFP-T2A-PURO.

Life cell imaging and Zetaview measurements

OCI-AML3 cells expressing GFP NAMPT had to be attached to a surface advance. For this, ibidi dishes were coated with recombinant retronectin (FN). Cells were counted and pre-treated with the indicated compounds in RPMI no phenol red for one hour in the incubator. 300.000 – 400.000 cells were plated in 2 ml RPMI no phenol red in the dishes. The cells were monitored at a Confocal Microscope Leica TCS SP8 X using the Argon laser for GFP signal. The GFP expressing cells were captured for 18 h, taking a picture every minute. Signal intensity was calculated using Fiji software and plotting the Z-axis profile. The cells were counted using the plugin cell counter. The Zetaview particle tracking system was used to determine particle concentration and size distribution of fluorescent particles in the supernatant of cultured cells. $2{,}5 \times 10^6$ OCI-AML3 cells expressing GFP NAMPT were cultured for 24 h in 1.2 ml RPMI no phenol red with the indicated compounds in a 24 well plate at 37°C. Measurement was performed without dilution.

Mouse experiments

All mouse experiments were conducted according to the national animal welfare law (Tierschutzgesetz) and were approved by the Regierungspräsidium Tübingen, Germany. For all experiments, NOD.Cg-Prkdc<scid>Il2rgytm1Wjl>/SzJ (NSG) strains were used. The NSG mice were irradiated sublethally (325 cGy) and injected with AML or normal HSPCs incubated with 2 mM peptides for 30 min under serum-free condition.

Statistics

All statistical analyses were performed using the GraphPad Prism 8 software using Ordinary one-way ANOVA.

Acknowledgments

The authors would like to thank all members of the Core Facility FACS and the animal facility of the University Ulm for breeding and maintenance of the animals.

Author Contributions

L.M.K., M.H., M.G., D.T. and V.P.S.R. performed research and analysed the data. J.M., D.S., E.H. contributed to data interpretation. L.M.K. and C.B. wrote the manuscript, C.B. designed the project. All authors have read and agreed to the published version of the manuscript.

Funding

The work was supported by grants from the DFG (SFB 1279 project B01 to C.B, and project A06 to M.H. and J.M.; SPP 1923 and the Heisenberg Programme to D.S.) and by a grant from the Baden-Württemberg Foundation to J.M.. M.H is member of the international Graduate school in Molecular Medicine Ulm.

Disclosure of conflicts of interest

J.M. and M.H. are coinventors on granted and filed patents that claim to use EPI-X4 and improved derivatives for therapy of CXCR4-linked diseases. The other authors declare no competing financial interests related to the work described.

References

1. Sriram K, Insel PA. G Protein-Coupled Receptors as Targets for Approved Drugs: How Many Targets and How Many Drugs? *Mol Pharmacol*. 2018;93(4):251-258.

2. Innamorati G, Valenti MT, Giovinazzo F, Carbonare LD, Parenti M, Bassi C. Molecular Approaches To Target GPCRs in Cancer Therapy. *Pharmaceuticals*. 2011;4(4):567-589.

3. Kaiser LM, Hunter ZR, Treon SP, Buske C. CXCR4 in Waldenstrom's Macroglobulinema: chances and challenges. *Leukemia*. 2021;35(2):333-345.

4. Rossi D, Zlotnik A. The biology of chemokines and their receptors. *Annu Rev Immunol*. 2000;18:217-242.

5. Chatterjee S, Behnam Azad B, Nimmagadda S. The intricate role of CXCR4 in cancer. *Adv Cancer Res*. 2014;124:31-82.

6. Kaiser LM, Hunter ZR, Treon SP, Buske C. CXCR4 in Waldenström's Macroglobulinema: chances and challenges *Leukemia*. 2020;in press.

7. Zeng Z, Shi YX, Samudio IJ, et al. Targeting the leukemia microenvironment by CXCR4 inhibition overcomes resistance to kinase inhibitors and chemotherapy in AML. *Blood*. 2009;113(24):6215-6224.

8. Burger JA, Peled A. CXCR4 antagonists: targeting the microenvironment in leukemia and other cancers. *Leukemia*. 2009;23(1):43-52.

9. Garten A, Schuster S, Penke M, Gorski T, de Giorgis T, Kiess W. Physiological and pathophysiological roles of NAMPT and NAD metabolism. *Nat Rev Endocrinol*. 2015;11(9):535-546.

10. Zirafi O, Kim KA, Standker L, et al. Discovery and characterization of an endogenous CXCR4 antagonist. *Cell Rep*. 2015;11(5):737-747.

11. Harms M, Habib MM, Nemska S, et al. An optimized derivative of an endogenous CXCR4 antagonist prevents atopic dermatitis and airway inflammation. *bioRxiv*. 2020:2020.2008.2028.272781.

12. Sun X, Huang S, Wang X, Zhang X, Wang X. CD300A promotes tumor progression by PECAM1, ADCY7 and AKT pathway in acute myeloid leukemia. *Oncotarget*. 2018;9(44):27574-27584.

13. Niavarani A, Herold T, Reyal Y, et al. A 4-gene expression score associated with high levels of Wilms Tumor-1 (WT1) expression is an adverse prognostic factor in acute myeloid leukaemia. *British journal of haematology*. 2016;172(3):401-411.

14. Grolla AA, Travelli C, Genazzani AA, Sethi JK. Extracellular nicotinamide phosphoribosyltransferase, a new cancer metabokine. *British journal of pharmacology*. 2016;173(14):2182-2194.

15. Kokkaliaris KD, Scadden DT. Cell interactions in the bone marrow microenvironment affecting myeloid malignancies. *Blood Advances*. 2020;4(15):3795-3803.

16. Goulard M, Dosquet C, Bonnet D. Role of the microenvironment in myeloid malignancies. *Cellular and molecular life sciences : CMLS*. 2018;75(8):1377-1391.

17. Waclawiczek A, Hamilton A, Rouault-Pierre K, et al. Mesenchymal niche remodeling impairs hematopoiesis via stanniocalcin 1 in acute myeloid leukemia. *The Journal of Clinical Investigation*. 2020;130(6):3038-3050.

18. Duarte D, Hawkins ED, Lo Celso C. The interplay of leukemia cells and the bone marrow microenvironment. *Blood*. 2018;131(14):1507-1511.

19. Uy GL, Rettig MP, Motabi IH, et al. A phase 1/2 study of chemosensitization with the CXCR4 antagonist plerixafor in relapsed or refractory acute myeloid leukemia. *Blood*. 2012;119(17):3917-3924.

20. Gail JR, Ellen KR, Yulia D, et al. Phase I trial of plerixafor combined with decitabine in newly diagnosed older patients with acute myeloid leukemia. *Haematologica*. 2018;103(8):1308-1316.

21. Peled A, Petit I, Kollet O, et al. Dependence of human stem cell engraftment and repopulation of NOD/SCID mice on CXCR4. *Science*. 1999;283(5403):845-848.

22. Broxmeyer HE, Orschell CM, Clapp DW, et al. Rapid mobilization of murine and human hematopoietic stem and progenitor cells with AMD3100, a CXCR4 antagonist. *J Exp Med*. 2005;201(8):1307-1318.

23. Wegner SA, Ehrenberg PK, Chang G, Dayhoff DE, Sleeker AL, Michael NL. Genomic organization and functional characterization of the chemokine receptor CXCR4, a major entry co-receptor for human immunodeficiency virus type 1. *The Journal of biological chemistry*. 1998;273(8):4754-4760.

24. Jourdan P, Vendrell J-P, Huguet M-F, et al. Cytokines and Cell Surface Molecules Independently Induce CXCR4 Expression on CD4⁺ CCR7⁺ Human Memory T Cells. *The Journal of Immunology*. 2000;165(2):716-724.

25. Gupta SK, Lysko PG, Pillarisetti K, Ohlstein E, Stadel JM. Chemokine receptors in human endothelial cells. Functional expression of CXCR4 and its transcriptional regulation by inflammatory cytokines. *J Biol Chem*. 1998;273(7):4282-4287.

26. Kalatskaya I, Berchiche YA, Gravel S, Limberg BJ, Rosenbaum JS, Heveker N. AMD3100 is a CXCR7 ligand with allosteric agonist properties. *Molecular pharmacology*. 2009;75(5):1240-1247.

27. Balabanian K, Lagane B, Infantino S, et al. The chemokine SDF-1/CXCL12 binds to and signals through the orphan receptor RDC1 in T lymphocytes. *J Biol Chem*. 2005;280(42):35760-35766.

28. Ramakrishnan R, Pena-Martinez P, Agarwal P, et al. CXCR4 Signaling Has a CXCL12-Independent Essential Role in Murine MLL-AF9-Driven Acute Myeloid Leukemia. *Cell Rep*. 2020;31(8):107684.

29. Kaiser LM, Harms M, Sauter D, et al. Targeting of CXCR4 by the Naturally Occurring CXCR4 Antagonist EPI-X4 in Waldenström's Macroglobulinemia. *Cancers*. 2021;13(4):826.

30. Demarest TG, Babbar M, Okur MN, et al. NAD+ Metabolism in Aging and Cancer. *Annual Review of Cancer Biology*. 2019;3(1):105-130.

31. Mitchell SR, Larkin K, Grieselhuber NR, et al. Selective targeting of NAMPT by KPT-9274 in acute myeloid leukemia. *Blood Adv*. 2019;3(3):242-255.

32. Cea M, Cagnetta A, Acharya C, et al. Dual NAMPT and BTK Targeting Leads to Synergistic Killing of Waldenstrom Macroglobulinemia Cells Regardless of MYD88 and CXCR4 Somatic Mutation Status. *Clin Cancer Res*. 2016;22(24):6099-6109.

33. Jones CL, Stevens BM, Pollyea DA, et al. Nicotinamide Metabolism Mediates Resistance to Venetoclax in Relapsed Acute Myeloid Leukemia Stem Cells. *Cell Stem Cell*. 2020.

34. Yoshida M, Satoh A, Lin JB, et al. Extracellular Vesicle-Contained eNAMPT Delays Aging and Extends Lifespan in Mice. *Cell Metab*. 2019;30(2):329-342 e325.

35. Yoon MJ, Yoshida M, Johnson S, et al. SIRT1-Mediated eNAMPT Secretion from Adipose Tissue Regulates Hypothalamic NAD+ and Function in Mice. *Cell Metab*. 2015;21(5):706-717.

Figures:

Fig.1: Expression of CXCR4 in functionally validated LSCs (A) Expression of CXCR4 in functionally validated LSCs (LMPP and GMP) vs CD34-negative non-LSCs. Shown is the median and range from 6 individual samples.

Fig. 2: EPI-X4 and its derivates block the CXCR4 epitope 12G5 and growth and CXCL12-directed transwell migration of AML cells. (A-B) Antibody competition assay shows blockage of the 12G5 epitope but no effect on the 1D9 epitope of OCI-AML3 cells by EPI-X4 and optimized derivatives. Mean values (± SEM) of five independent experiments are shown. (C) Colony formation assay of OCI-AML3 cells counted after 7 days. Shown are the mean number of colonies (± SEM) of 3 independent experiment performed in duplicates under experimental conditions as indicated. Unpaired t-test *p<0,05. (D-E) Shown are the mean number of migrated cells relative to CXCL12-only treated cells and an inactive control. (D) Treatment with an equimolar concentration of 200 µM and (E) 10 µM (unpaired t-test **p<0.01; The ordinary one-way ANOVA and Dunnetts multiple comparison test **< 0.01; *<0.05; ns=not significant). Mean values (± SEM) of three independent experiments performed in duplicates are shown.

Fig. 3: EPI-X4 and its optimized derivatives reduce homing and engraftment of primary human AML cells but not of normal HSCs in NSG mice (A**)** Reduced BM homing of cells treated with EPI-X4, WSC02 or JM#21. The figure shows percentage of CD45+ cells 20 h after transplantation relative to the number of injected cells. Cells originating from one patient were transplanted into independent different cohorts of mice (n=3 per experimental arm). (*p<0.05; **< 0.01; using ordinary one-way ANOVA and Dunnetts multiple comparison test). (B) Level of human engraftment in NSG mice 12 weeks after transplantation. Engraftment is reduced in mice which received patient cells treated *in vitro* with peptides as indicated compared to the inactive peptide control (n=3 or 4 per experimental arm) (***p<0.001). (C) Engraftment of normal CD34+ HSPCs is not changed upon treatment with the different peptides compared to

the inactive peptide control (n=2). Dots are presenting individual mice transplanted with primary AML cells or normal HSPCs.

Figure 4. Inhibition of ERK and AKT signaling by EPI-X4 and its optimized derivatives. Cells were first stimulated with 100 ng/ml CXCL12 and subsequently incubated with the different peptides. Levels of phosphorylated ERK (A) and phosphorylated AKT (B) was determined by intracellular flow cytometry. Shown are data derived from 3 individual experiments performed in triplicates ± SEM. Fold change is indicated comparing signal intensity between stimulated sample (CXCL12) and unstimulated control (PBS) (MFIstim/MFIunstim).

Fig. 5. Kinomic changes in MAPK signaling of EPI-X4 treated AML cells. Relative kinase activity in EPI-X4 treated vs. untreated OCI-AML3 cells. Kinases were ranked using a combined score based on a sensitivity score indicating group difference and specificity score derived for a set of peptides related to the respective kinase. Shown are candidates with a relative kinase activity of -0.25 compared to untreated cells including top candidates related to the MAPK pathway with p38 (delta), p38 (beta) and ERK family members 1, 2 and 5 (A) and top candidates with a specificity-score of < 1.3 (B). (C) Kinome tree shows STK and PTK kinases affected by EPI-X4. TK (Tyrosine Kinase), TKL (Tyrosine Kinase-Like), STE (Homologs of the yeast STE7, STE11 and STE20 genes), CK1 A (Cell Kinase), AGC (Protein Kinase A, G, and C families (PKA, PKC, PKG)), CAMK (Calmodulin/Calcium regulated kinases), CMGC (set of families (CDK, MAPK, GSK3 and CLK) and atypical protein kinases.

Fig. 6. Altered gene expression profile induced by EPI-X4. (A) Pathway analysis of differentially expressed genes upon EPI-X4 treatment compared to inactive peptide control (FDR<0,05). Gene set enrichment tools of Enrichr http://amp.pharm.mssm.edu/Enrichr/) were used for the analyses. All gene sets were filtered with an adjusted p-value <0.05. (B) Schematic overview of metabolic genes affected by EPI-X4 treatment in AML cells. Downregulated metabolites are highlighted in green. *SLC2A3* (Solute Carrier Family 2 Member 3) is important for glucose uptake. Downregulated key regulators in glycolysis from glucose to pyruvate: *HK1*

(Hexokinase 1), *PFKM* (Phosphofructokinase, Muscle), *ALDOC* (Aldolase, Fructose-Bisphosphate C), *TPI1* Triosephosphate Isomerase 1, *PGM* (Phosphoglucomutase), *ENO1/2* (Enolase 1/2), *PKM* Pyruvate Kinase M1/2). *LDH A/B* (Lactate Dehydrogenase A/B) converts L-lactate to pyruvate in the final step of anaerobic glycolysis. The pyruvate dehydrogenase (PDH) complex is the primary link between glycolysis and the tricarboxylic acid (TCA) cycle. *ACAT* (Acetyl-CoA Acetyltransferase 1) catalyzes the formation of acetoacetyl-CoA from two molecules of acetyl-CoA. Glutamate metabolism: *IDH1* (Isocitrate dehydrogenases) catalyzes reaction from isocitrate to 2-oxoglutarate. Genes involved in lipid synthesis: *ACSS2* (Acyl-CoA Synthetase Short Chain Family Member 2) converts acetate to acetyl-CoA, ACACA (Acetyl-CoA Carboxylase Alpha), *SCD* (Stearoyl-CoA Desaturase), *FADS* 1/2 (Fatty Acid Desaturase 1/2). Genes involved in cholesterol biosynthesis: *ACLY* (ATP Citrate Lyase) catalyzes formation of acetyl-CoA from citrate, (ACAT Acetyl-CoA Acetyltransferase), *HMGCS1* (3-Hydroxy-3-Methylglutaryl-CoA Synthase 1), *HMGCR* (3-Hydroxy-3-Methylglutaryl-CoA Reductase).

Fig. 7. Proteomic changes of AML cells upon EPI-X4 treatment. Differentially expressed proteins in AML cells incubated with EPI-X4 vs. inactive control. Enrichr analysis of significantly (A) downregulated proteins and (B) upregulated proteins. All differentially expressed proteins with FDR<0.05, FC>2.

Fig. 8. EPI-X4 reduces intracellular NAMPT in AML cells. (A) Volcano plot reflecting results of proteome analysis. Fold-changes of control versus EPI-X4 treatment are shown on the x axis and statistical significance (-log10 of p value) is shown on the y axis. Statistical analysis was performed by Student t-test, the dashed line separates colored points with $p < 0.05$. Dots having a fold-change less than 2 (log2 = 1) are shown in gray. Red dots are downregulated proteins, blue dots are upregulated. (B) Western blot showing NAMPT protein of OCI-AML3 cells treated with EPI-X4 (concentration 200 µM), optimized WSC02 and JM#21 (concentration 10 µM) as well as the inactive control (200 µM), AMD3100 and the NAMPT Inhibitor FK-866 as control (concentration 10 µM) for 24 h. The experiment was performed in triplicates, shown

is one representative blot. (C) Graph shows percent of band volumes of the Western blot, performed with AML cells treated with the indicated compounds. The NAMPT protein was monitored over 22 h. D) NAMPT western blot of AML cells treated with inactive (200 µM) peptide or EPI-X4 (200 µM) plus/minus recombinant NAMPT. (E) Western blot showing NAMPT protein of CD34+ normal HSPCs treated with EPI-X4 (concentration 200 µM), optimized WSC02 and JM#21 (concentration 10 µM) as well as the inactive control (200 µM), AMD3100 and a NAMPT Inhibitor FK-866 (concentration 10 µM) for 24 h. (F) Real time intensity blot analysis of viable OCI-AML3 cells overexpressing GFP and NAMPT. Cells are untreated or treated with EPI-X4, JM#21 or the inactive peptide control and analyzed by life cell imaging. GFP Intensity signal of the indicated cell number is captured every minute for 18 h. Values are determined using Fiji analysis software and blotted as percent reduction. (G) visualization of fluorescent particles in cell culture media of AML cells treated with the different components, tracked by videomicroscope (Zetaview). Supernatant of AML cells treated with the indicated Peptides Inactive (200 µM), EPI-X4 (200 µM) and JM#21 (10 µM) was analyzed after 24h. ANOVA and Dunnetts multiple comparison test (****p<0.0001)

Fig.1. CXCR4 expression in functionally validated LSCs

A)

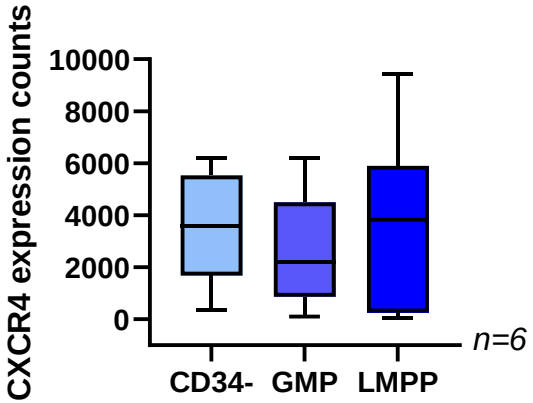

Fig. 2 EPI-X4 and its derivatives block the CXCR4 receptor and impair growth and migration of AML cells

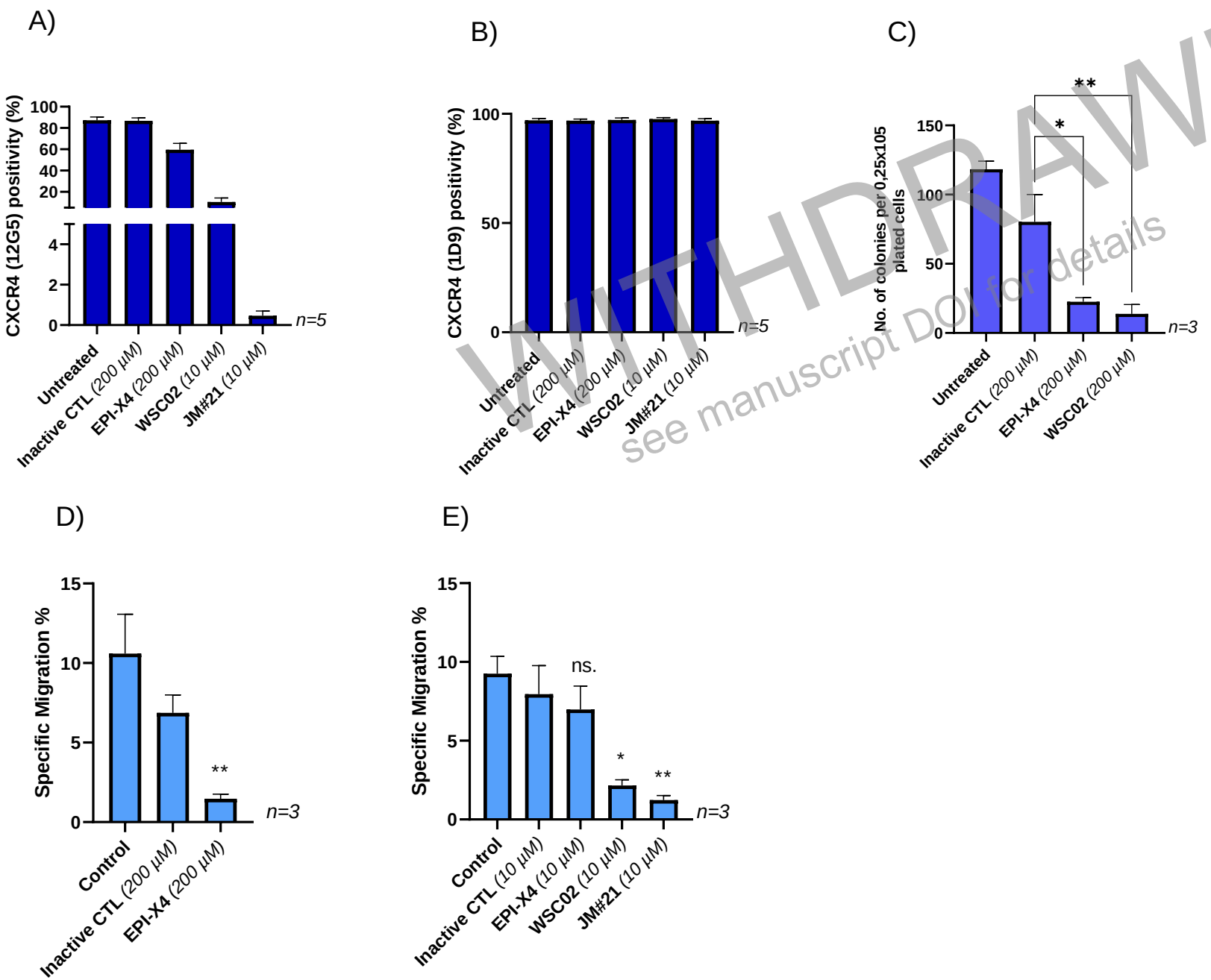

Fig. 3 EPI-X4 and its optimized derivatives reduce homing and engraftment of primary human AML cells but not of normal HSCs in NSG mice

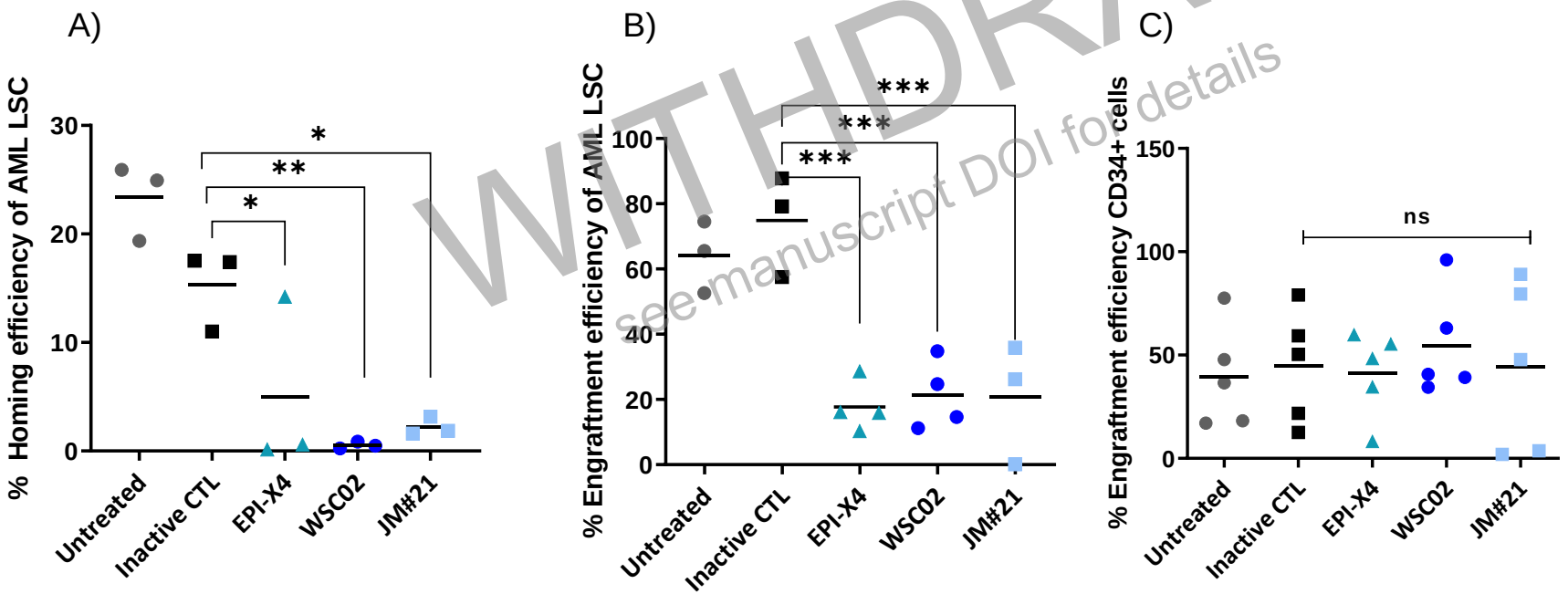

Fig. 4 Inhibition of ERK and AKT signaling by EPI-X4 and its optimized derivatives

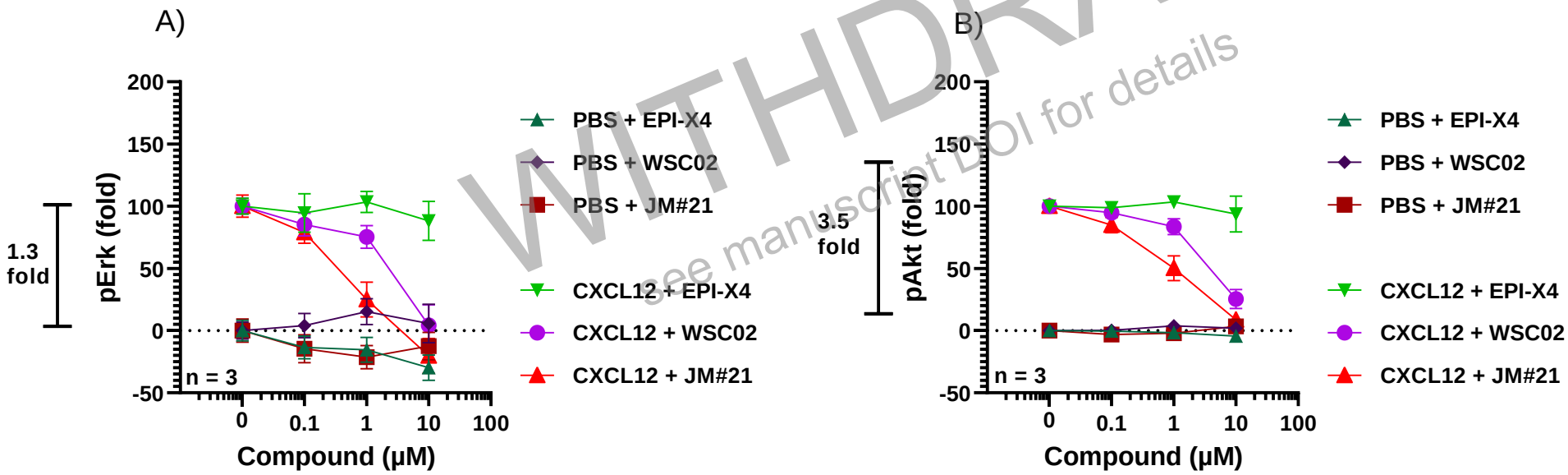

Fig.5 Kinome of EPI-X4 treated AML cells

A)

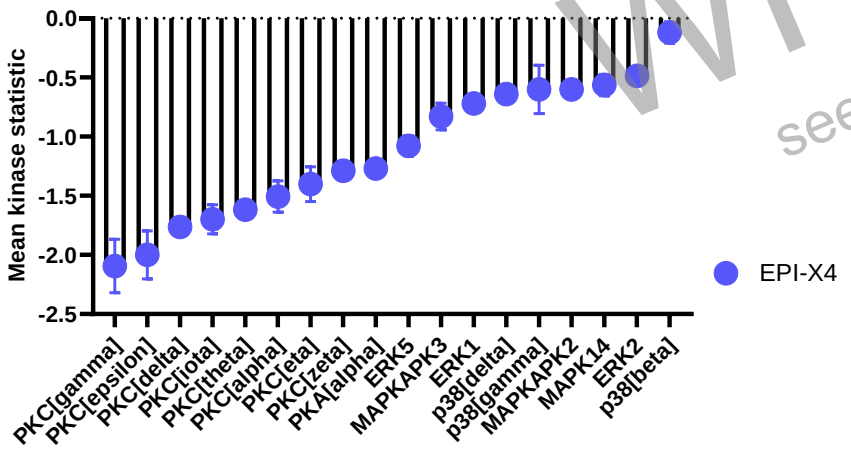

B)

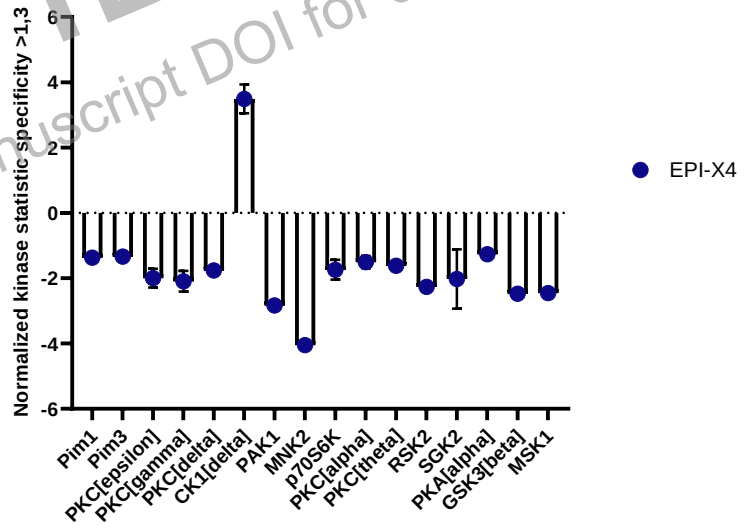

C)

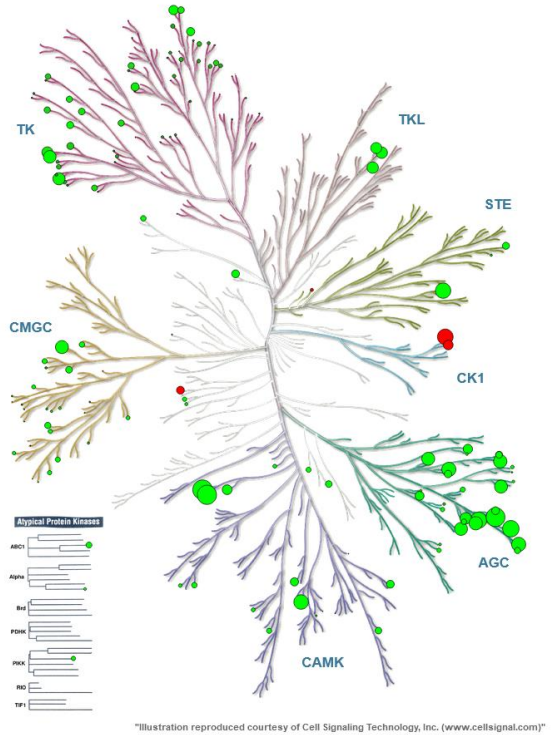

Fig. 6 Altered gene expression profile in OCI-AML3 cells induced by EPI-X4

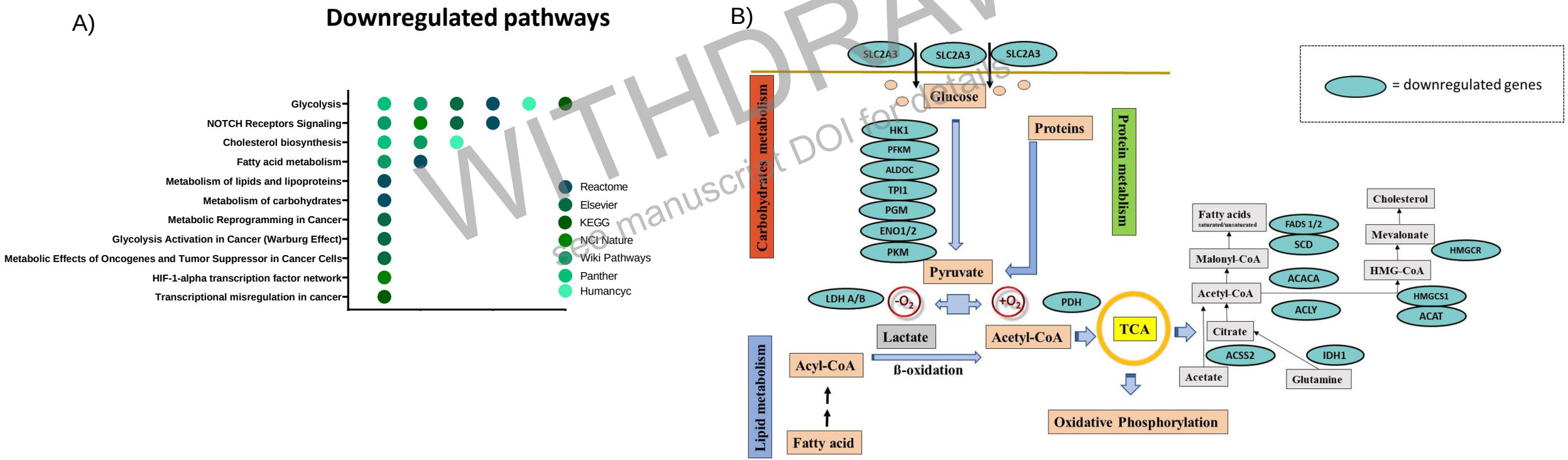

Fig. 7. Altered protein expression profile in OCI-AML3 cells induced by EPI-X4

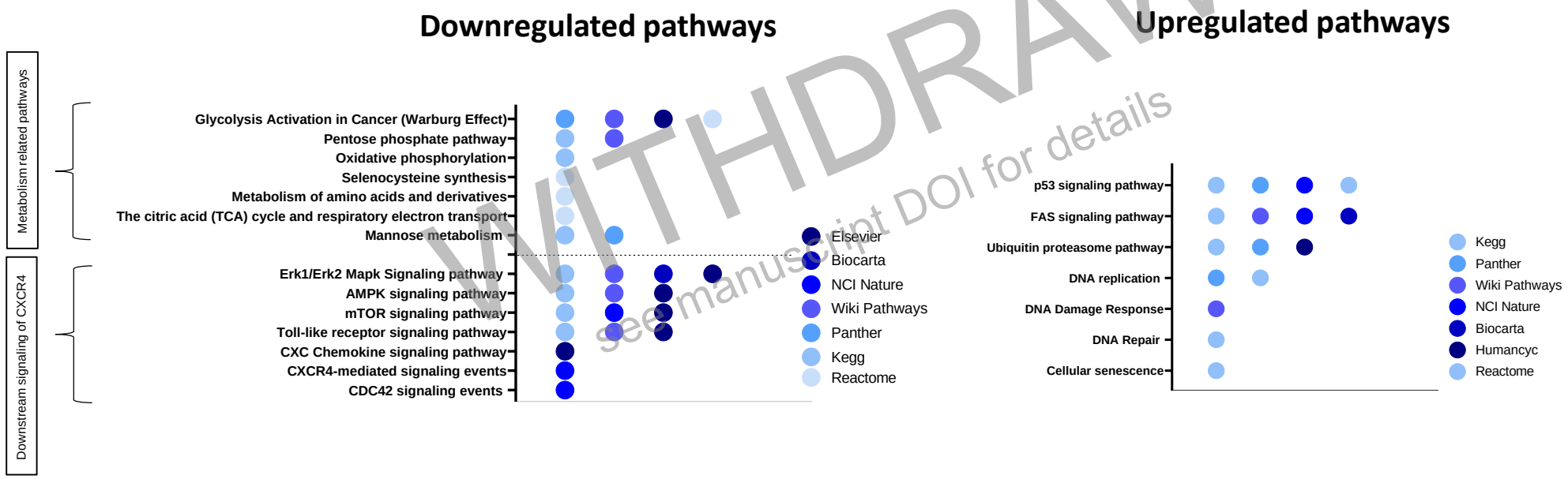

Fig. 8 EPI-X4 reduces intracellular NAMPT in AML cells

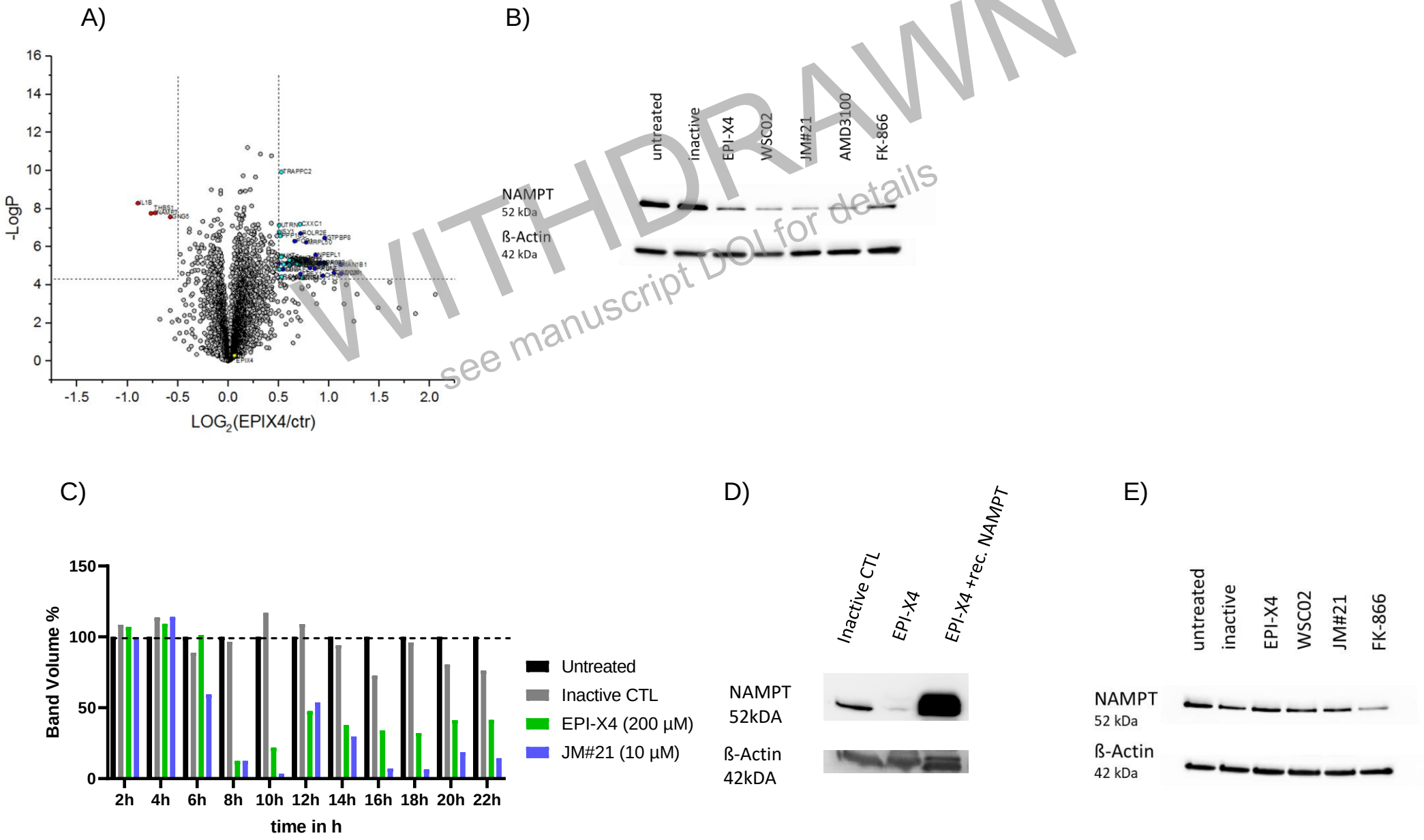

Fig. 8 EPI-X4 reduces intracellular NAMPT in AML cells